Supporting Information for:

Synergistic effect of multivalent Ti, Zr, and oxygen vacancies to significantly enhance the hydrogen sorption properties of MgH_2

*Fanqi Bu [a], Ali Wajid [b], Mengyue Gu [a], Ting Liu [c], Siyuan Liu [a], Xin Ji [a], Xin Liu [a], Shujiang Ding [b], Yonghong Cheng [a], Jinying Zhang [a] **

[a] *State Key Laboratory of Electrical Insulation and Power Equipment, Center of Nanomaterials for Renewable Energy (CNRE), School of Electrical Engineering, Xi'an Jiaotong University, Xi'an, Shaanxi, 710049, PR China*

[b] *School of Chemistry, Xi'an Key Laboratory of Sustainable Energy Materials Chemistry, State Key Laboratory for Mechanical Behavior of Materials, Xi'an Jiaotong University, Xi'an 710049, China*

[c] *Aviation Engineering school, Air Force Engineering University, Xi'an 710038, China*

** Corresponding author: Email：jinying.zhang@mail.xjtu.edu.cn*

Material characterizations

Transmission electron microscopy (TEM) images, high-resolution TEM (HRTEM) images, high-angle annular dark-field scanning transmission electron microscopy (HAADF-STEM) and elemental mapping were acquired by Lorenz Transmission Electron Microscope (Talos F200X). Scanning electron microscopy (SEM) images were recorded by Quanta 250FEG equipment. X-ray diffraction (XRD) patterns were obtained from a Bruker D2 PHASER using Cu/Kα radiation (λ =1.5418Å) at 40 kV and 30 mA. X-ray photoelectron spectroscopy (XPS) spectra were obtained using a Thermo Fisher ESCALAB spectrometer. The deposited thickness of amorphous ZrO_2 was obtained by ellipsometry (SE401adv-C, SENTECH, Germany). The hydrogen storage properties of MgH_2-based materials were tested using a homemade HPSA-auto apparatus.[1] Temperature programmed desorption (TPD) was tested from 100°C to 400°C at a rate of 3 °C/min. The isothermal desorption kinetic properties of the samples were tested at different temperatures (225, 250, 275, and 300°C) under starting hydrogen pressures below 0.05 bar. Similarly, the isothermal hydrogen absorption kinetic properties of the samples were tested at different temperatures (20, 50, 100, and 150°C) under 30 bar H_2. The isothermal dehydrogenation (0.05 bar H_2) and rehydrogenation (30 bar H_2) tests of the samples were performed repeatedly at 275°C for the cycling test.

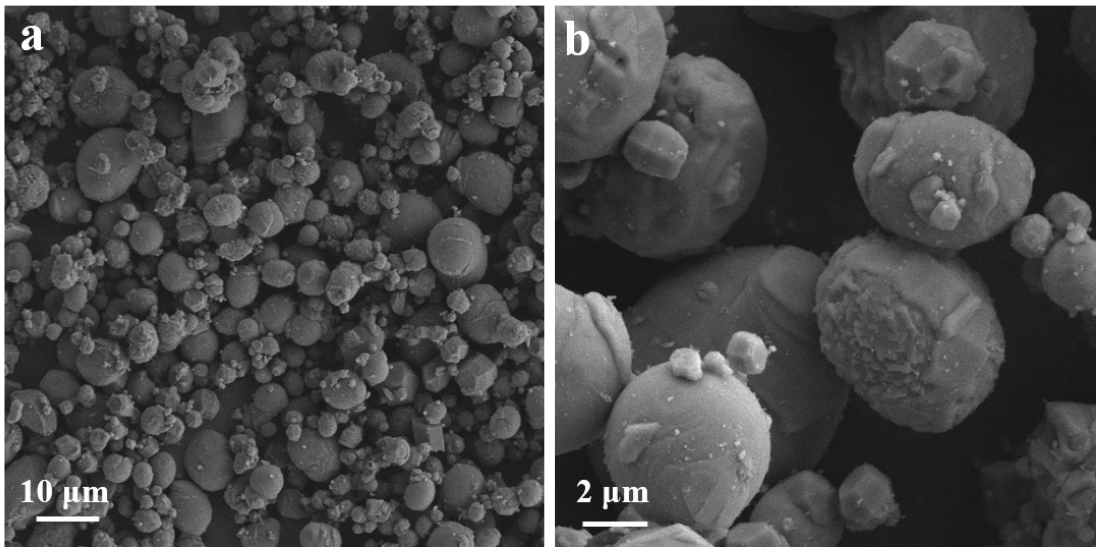

Figure S1 SEM images of commercial MgH_2 at different scales.

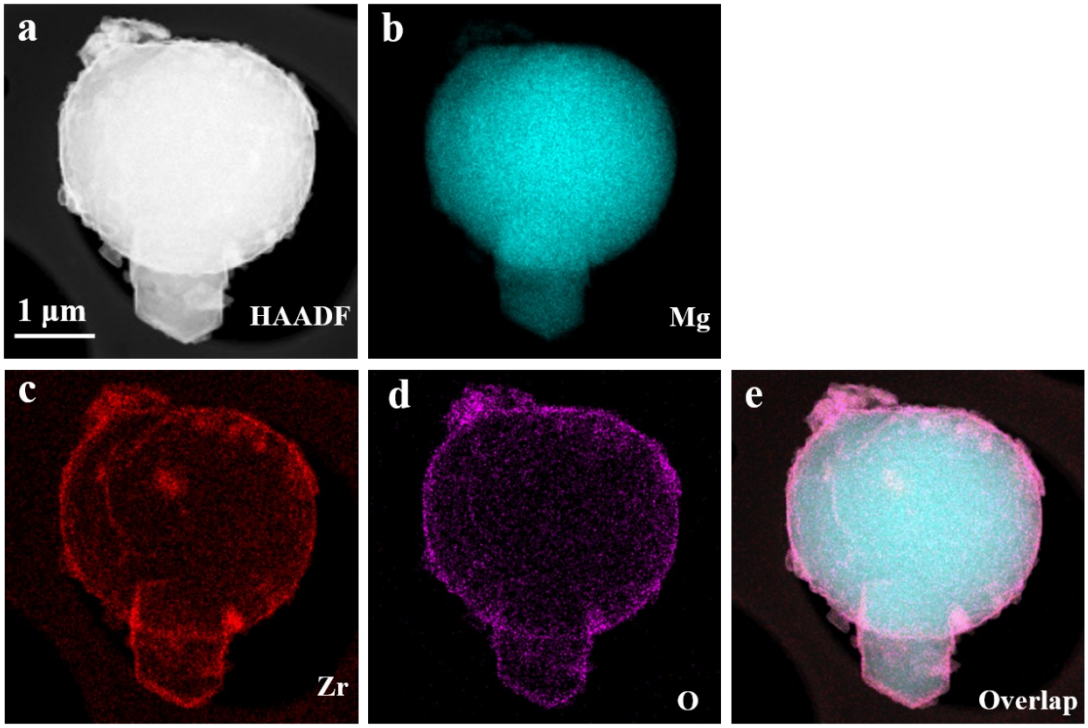

Figure S2 HAADF-STEM images of MgH_2@20nmZrO_2 with corresponding EDS elemental mapping analysis.

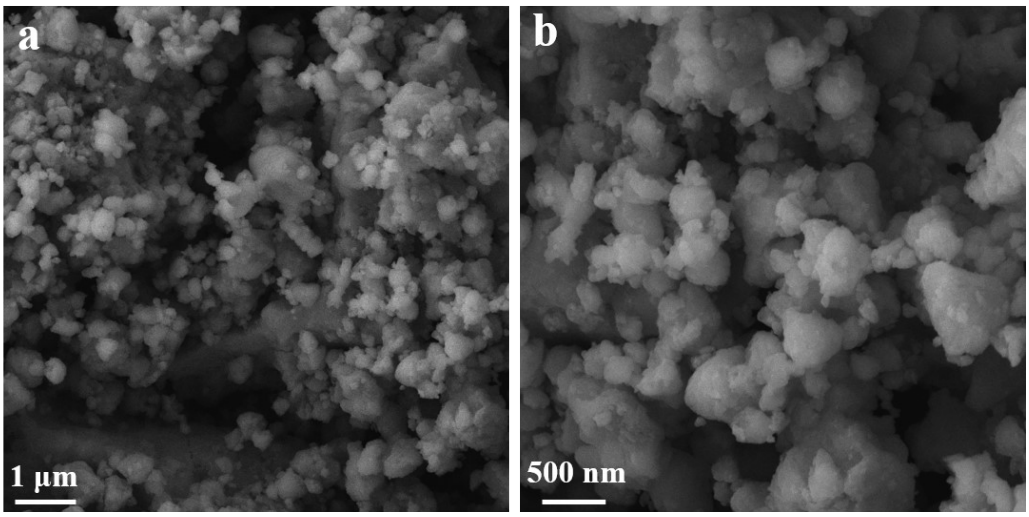

Figure S3 SEM images of MgH_2-20nmZrO_2 at different scales.

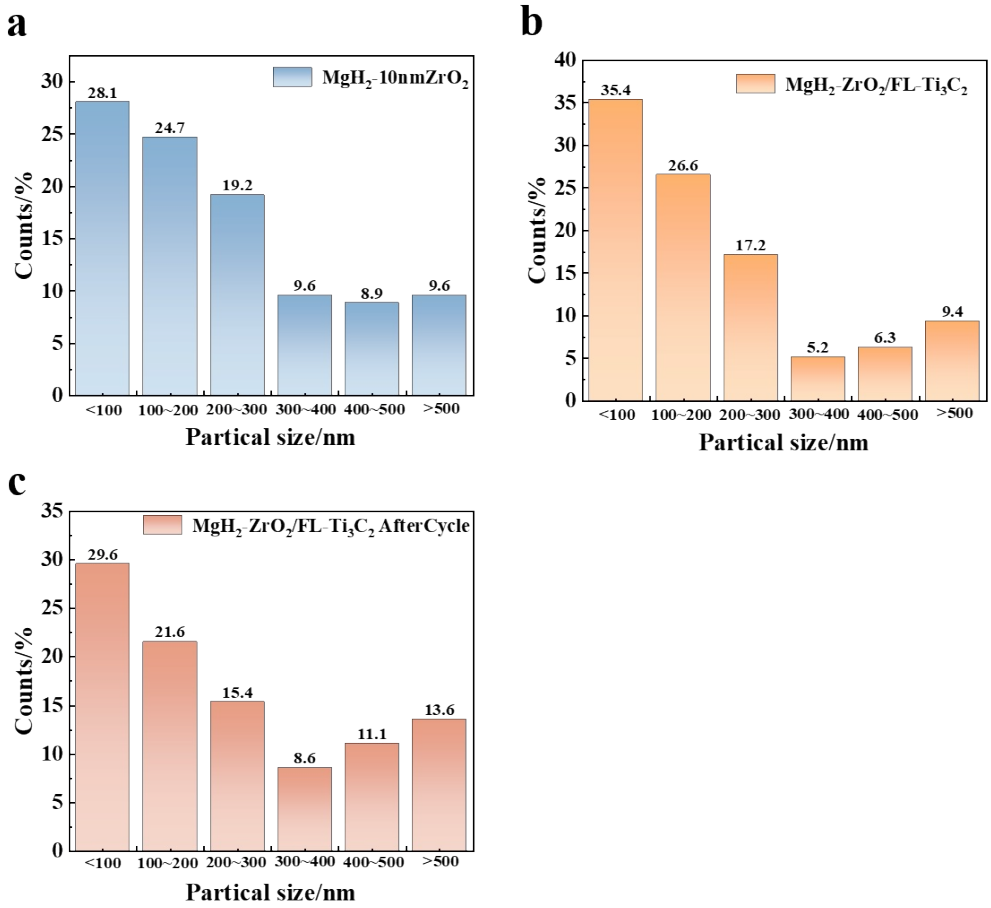

Figure S4 Particle size distribution of (a) MgH_2-10nmZrO_2, (b) pristine MgH_2-ZrO_2/FL-Ti_3C_2, and (c) MgH_2-ZrO_2/FL-Ti_3C_2 after 50 cycles.

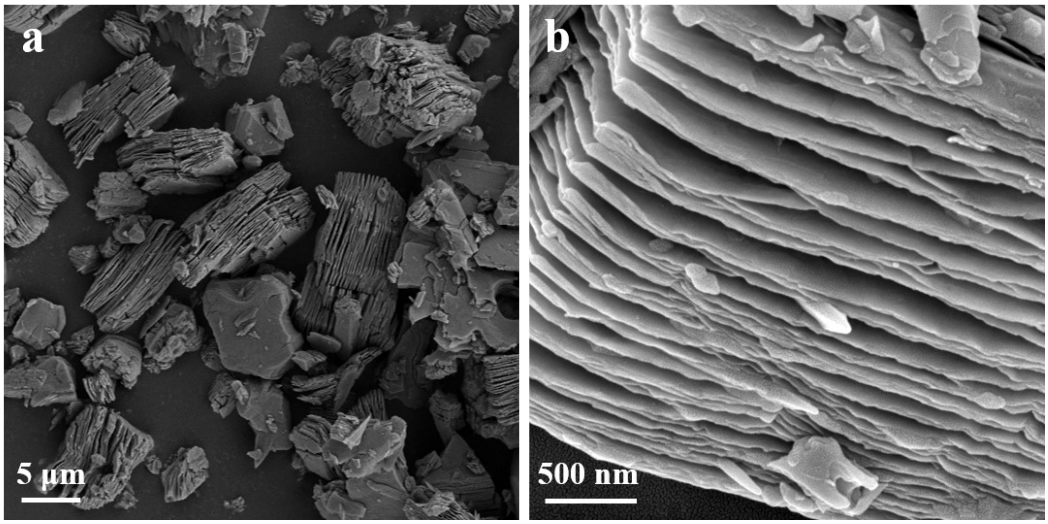

Figure S5 SEM images of untreated Ti_3C_2 at different scales.

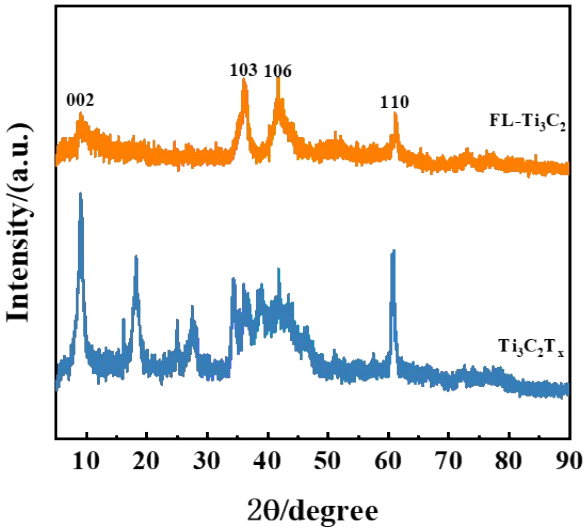

Figure S6 XRD patterns of Ti_3C_2 (blue) and FL-Ti_3C_2 (orange).

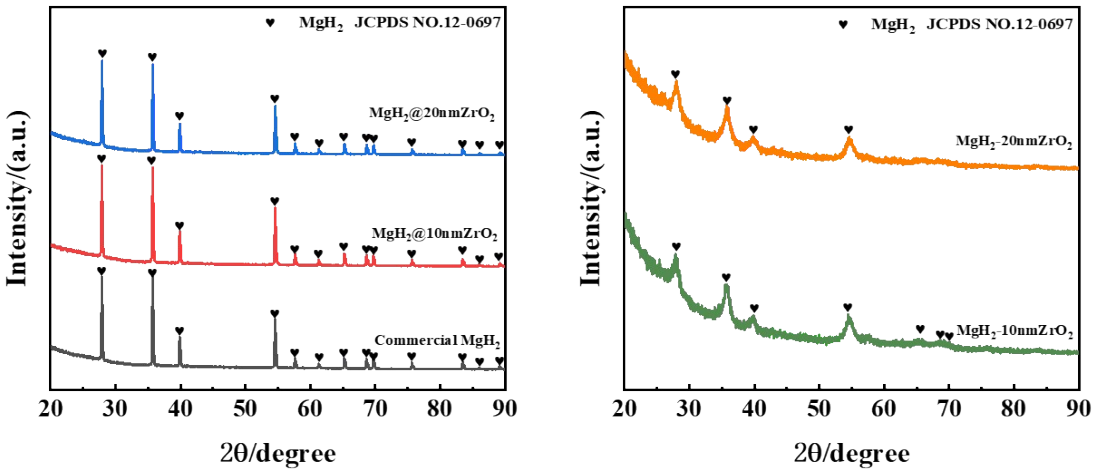

Figure S7 XRD patterns of (a) Commercial MgH_2, MgH_2@ZrO_2 and (b) MgH_2-ZrO_2.

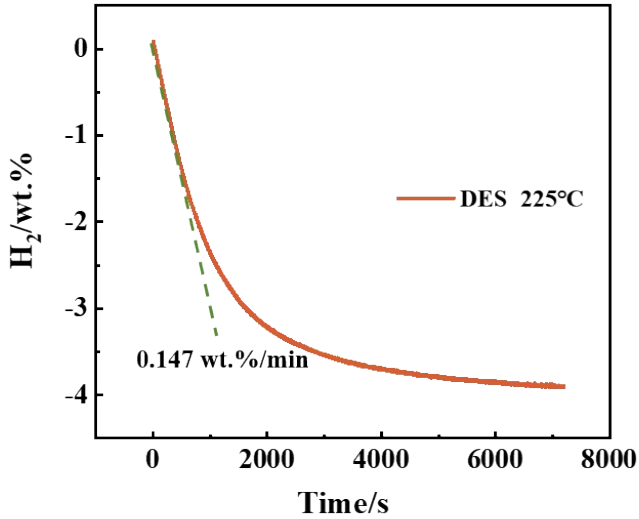

Figure S8 The isothermal dehydrogenation curve of MgH_2-ZrO_2/FL-Ti_3C_2 at 225℃.

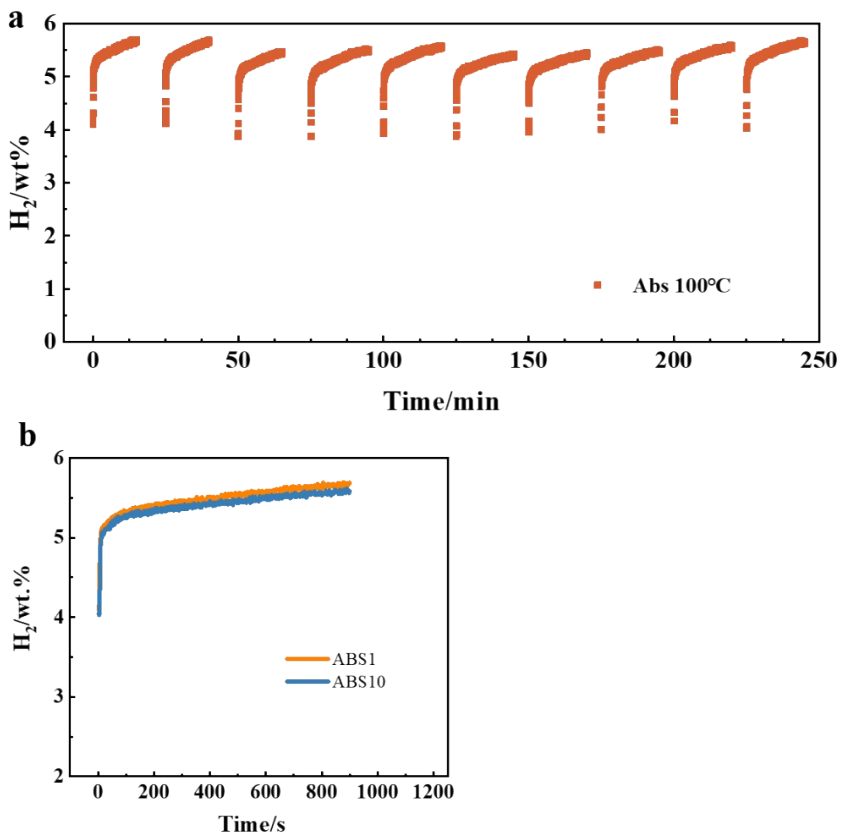

Figure S9 (a)The rehydrogenation cycle curves and (b) the comparison of the 1_{st} and 10_{th} rehydrogenation properties of MgH_2-ZrO_2/FL-Ti_3C_2 at 100°C.

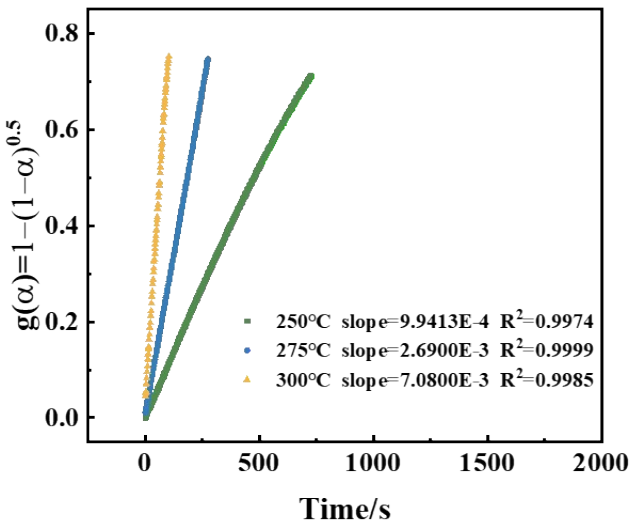

Figure S10 Time dependence of R2 modeling equation g(α) for MgH_2-ZrO_2/FL-Ti_3C_2 at different temperatures.

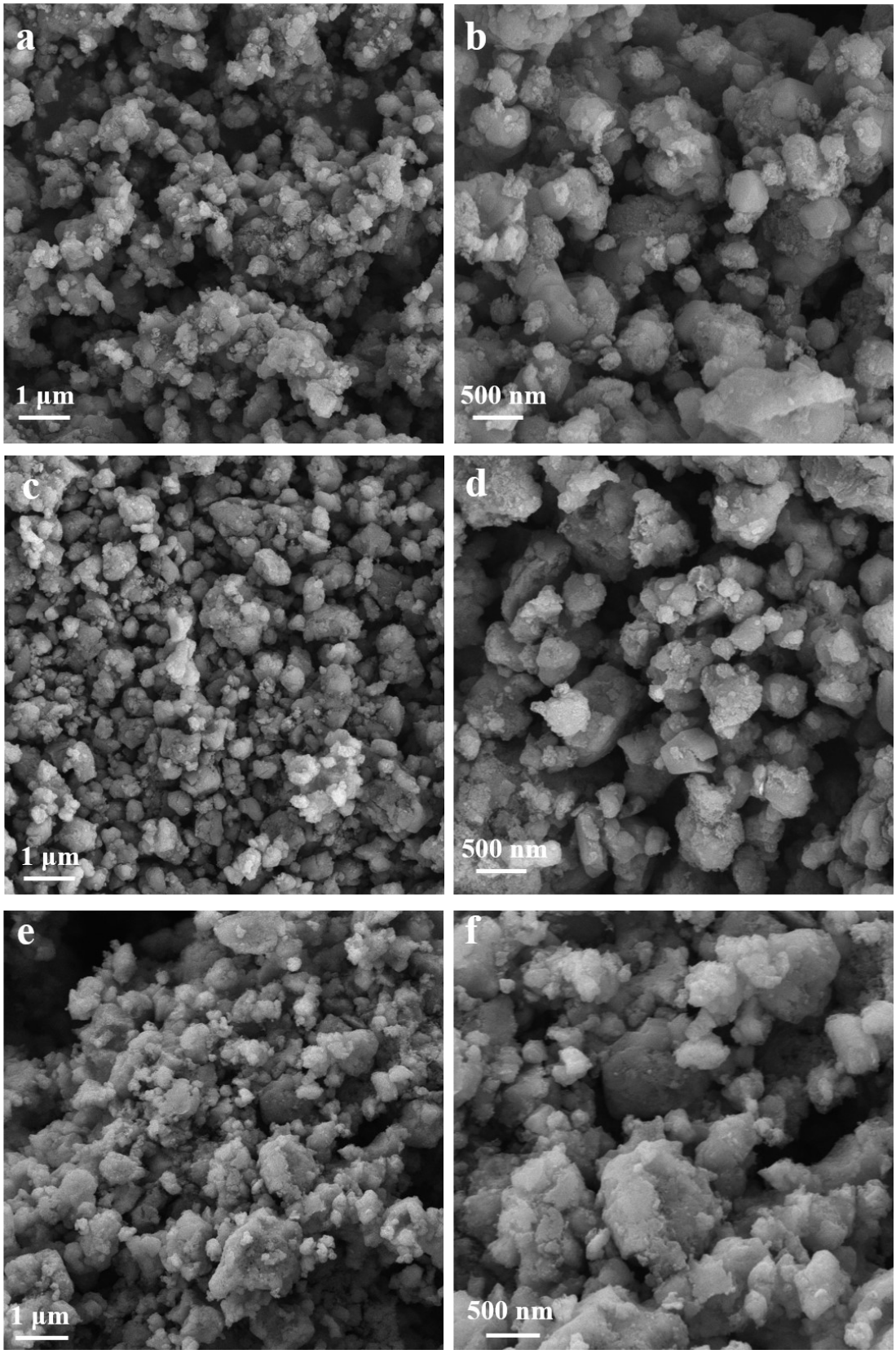

Figure S11 SEM images of MgH_2-ZrO_2/FL-Ti_3C_2 after (a, b) dehydrogenation, (c, d) rehydrogenation, and (e, f) 50 cycles at different scales.

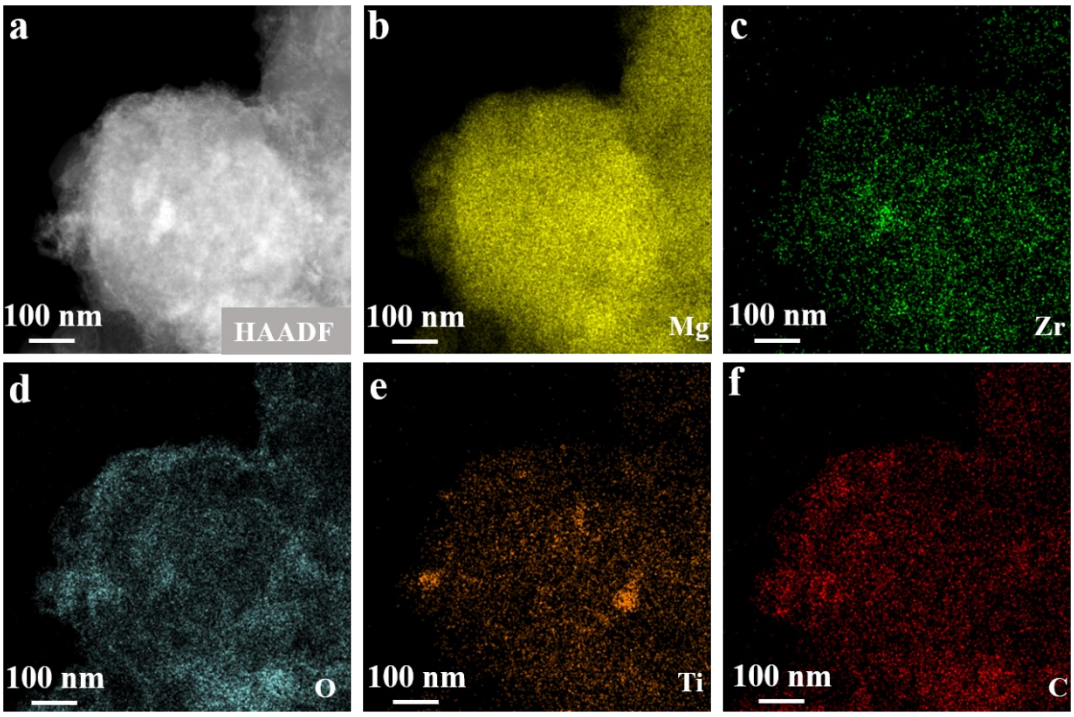

Figure S12 HAADF-STEM image of MgH_2-ZrO_2/FL-Ti_3C_2 after dehydrogenation reaction with corresponding EDS elemental mapping analysis.

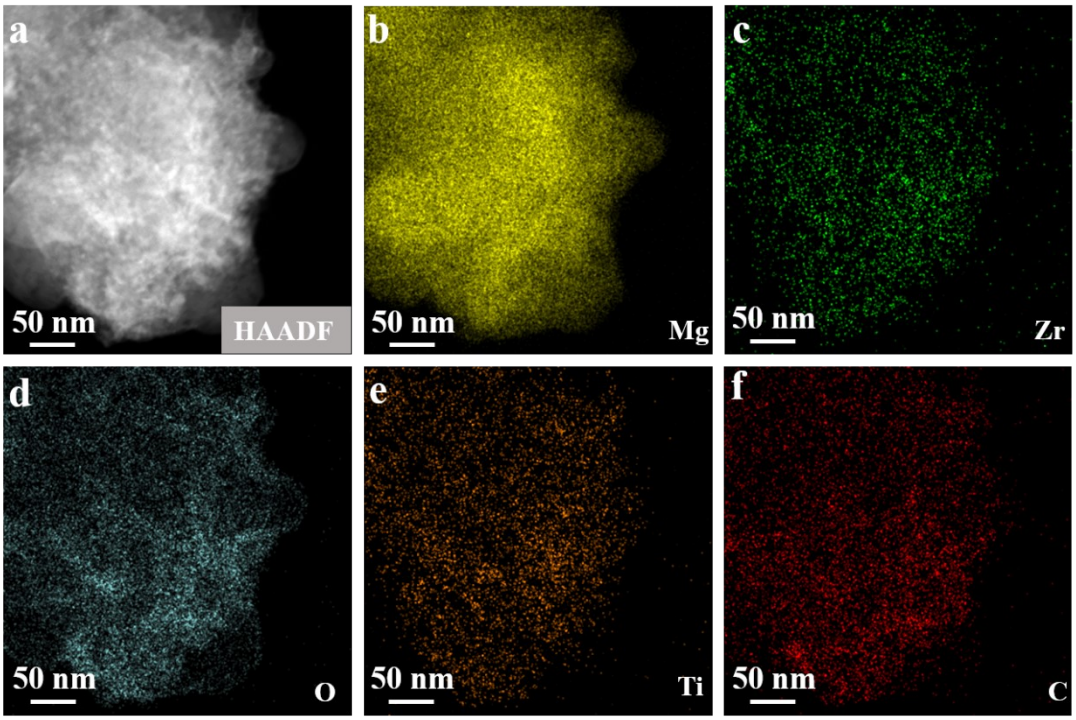

Figure S13 HAADF-STEM image of MgH_2-ZrO_2/FL-Ti_3C_2 after re-hydrogenation reaction with corresponding EDS elemental mapping analysis.

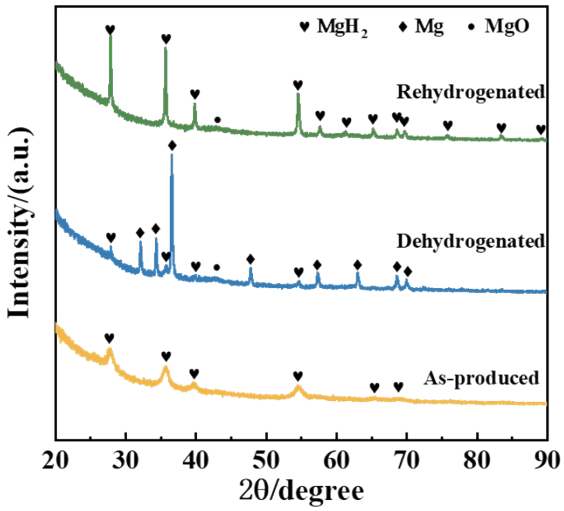

Figure S14 XRD patterns of the as-produced (yellow), dehydrogenated (blue), and re-hydrogenated (green) MgH_2-ZrO_2/FL-Ti_3C_2.

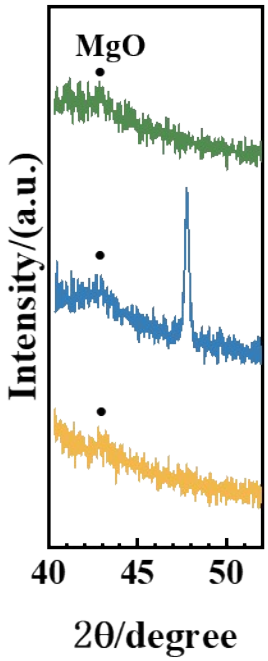

Figure S15 XRD patterns of the as-produced (yellow), dehydrogenated (blue), and rehydrogenated (green) MgH_2-ZrO_2/FL-Ti_3C_2 between 40° and 54°.

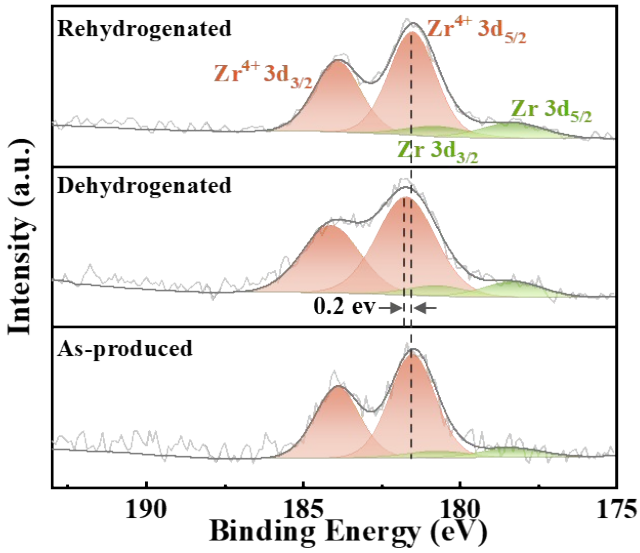

Figure S16 High-resolution Zr 3*d* spectra of the as-produced, dehydrogenated, and rehydrogenated MgH_2-ZrO_2/FL-Ti_3C_2 .

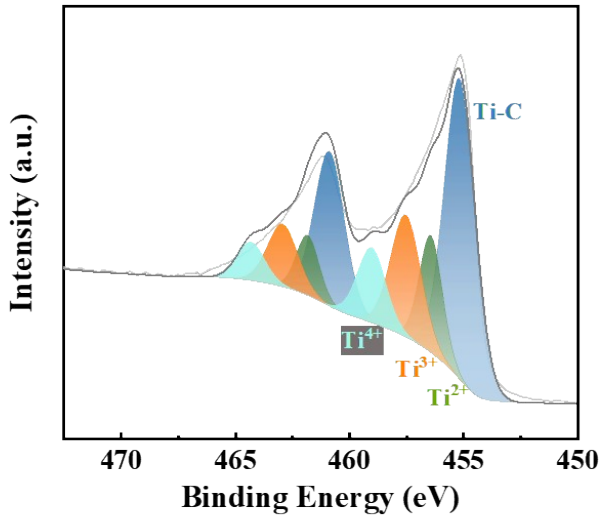

Figure S17 High-resolution Ti 2*p* spectra of the FL-Ti_3C_2.

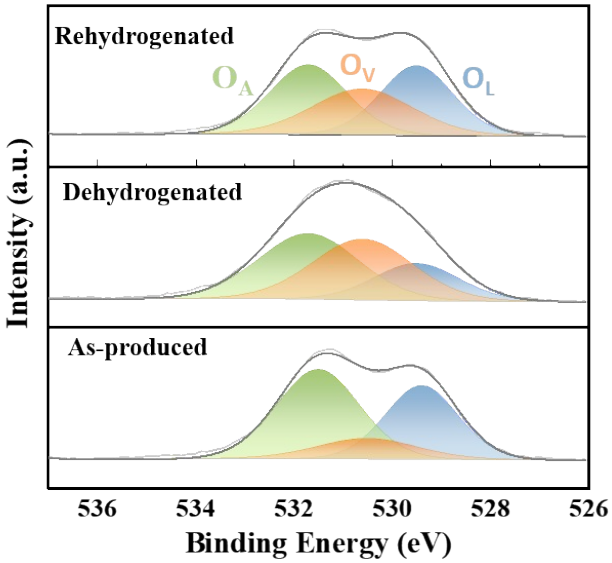

Figure S18 High-resolution O 1*s* spectrum of the as-produced, dehydrogenated, and rehydrogenated MgH_2-ZrO_2/FL-Ti_3C_2.

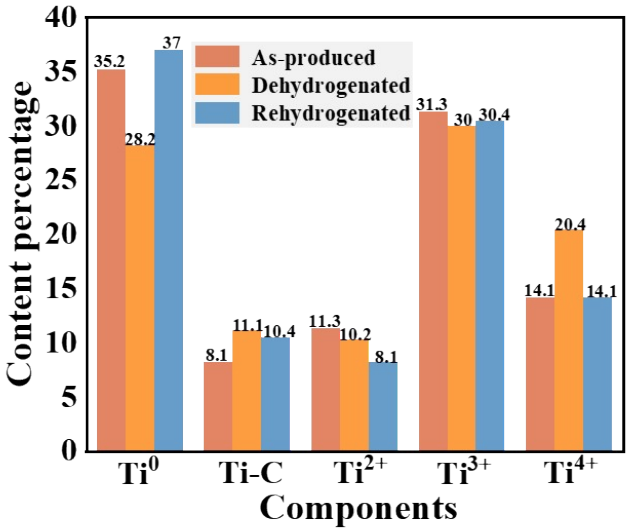

Figure S19 The proportion of peak area integrals corresponding to different Ti valence states of as-produced, dehydrogenated, and rehydrogenated MgH_2-ZrO_2/FL-Ti_3C_2.

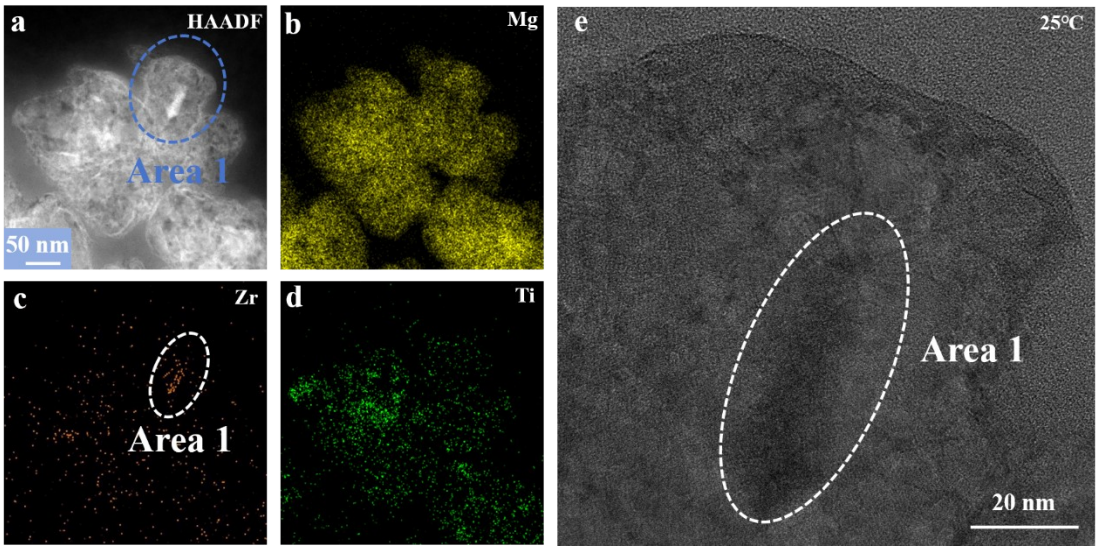

Figure S20 (a-d) HAADF-STEM image of MgH_2-ZrO_2/FL-Ti_3C_2 before in-situ pyrolysis characterization with corresponding EDS elemental mapping analysis. (e) HRTEM image obtained by zooming in on Area 1 of Figure S20a.

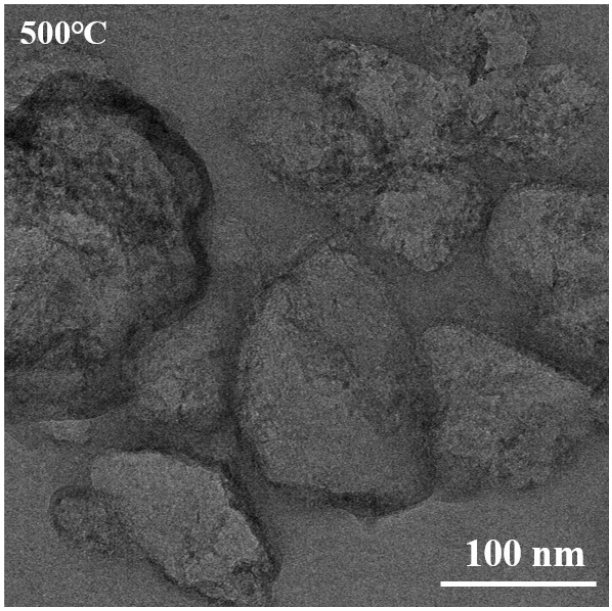

Figure S21 In-situ pyrolysis HRTEM image of MgH_2-ZrO_2/FL-Ti_3C_2 at 500℃.

Table S1 The detailed proportion of peak area integrals for different Ti valence states of as-produced, dehydrogenated, and rehydrogenated MgH_2-ZrO_2/FL-Ti_3C_2.

Sample	Ti valence	Normalized area integral	Proportion of area
dehydrogenated	Ti^0	0.94	28.2%
	Ti-C	0.37	11.1%
	Ti^{2+}	0.34	10.2%
	Ti^{3+}	1	30.0 %
	Ti^{4+}	0.68	20.4%
Rehydrogenated	Ti^0	1	37.0 %
	Ti-C	0.28	10.4%
	Ti^{2+}	0.22	8.1%
	Ti^{3+}	0.82	30.4%
	Ti^{4+}	0.38	14.1%
as-produced	Ti^0	1	35.2%
	Ti-C	0.23	8.1%
	Ti^{2+}	0.32	11.3%
	Ti^{3+}	0.89	31.3%
	Ti^{4+}	0.4	14.1%

Reference:

1. C. Wu, Y. Wang, Y. Liu, W. Ding and C. Sun, *Catalysis Today*, 2018, **318**, 113-118.